Biochemical Pharmacology 117 (2016) 68–77

Contents lists available at ScienceDirect

Biochemical Pharmacology

journal homepage: www.elsevier.com/locate/biochempharm

Pharmacological properties of microneurotrophin drugs developed for treatment of amyotrophic lateral sclerosis

James P. Bennett Jr. [a,b,c,d,*], Laura C. O'Brien [a,b], David G. Brohawn [a,e]

[a] Parkinson's Disease Research Center, Virginia Commonwealth University, Richmond, VA, United States
[b] Department of Physiology and Biophysics, Virginia Commonwealth University, Richmond, VA, United States
[c] Department of Neurology, Virginia Commonwealth University, Richmond, VA, United States
[d] Neurodegeneration Therapeutics, Inc., Charlottesville, VA, United States
[e] Department of Human Genetics, Virginia Commonwealth University, Richmond, VA, United States

ARTICLE INFO

Article history:
Received 26 May 2016
Accepted 1 August 2016
Available online 3 August 2016

Keywords:
Microneurotrophin
ALS
iPSC-derived motor neuron
RNA-sequencing
Gene ontology

ABSTRACT

Microneurotrophins (MNT's) are small molecule derivatives of dehydroepiandrosterone (DHEA) and do not have significant interactions with sex steroid receptors. MNT's retain high-affinity binding to protein tyrosine kinase (Trk) receptors and can mimic many pleiotropic actions of neurotrophin (NT) proteins on neurons. MNT's offer therapeutic potential for diseases such as amyotrophic lateral sclerosis (ALS) where motor neurons (MN) degenerate.

MNT's cross artificial membranes mimicking the blood–brain barrier, are not major substrates for ABC (ATP-binding cassette) transporters and are metabolized rapidly by mouse but more slowly by human hepatocytes. A lead MNT (BNN27) and its mono-oxidation metabolites enter mouse brain rapidly. RNA-sequencing measured gene expression profiles of human H9eSC-(embryonic stem cell)-derived or CTL (control) subject iPSC-(induced pluripotential stem cell)-derived MN's exposed to NT proteins or MNT molecules. Expression ratios (relative to DMSO (dimethylsulfoxide) vehicle) were calculated, and the resulting top 500 gene lists were analyzed for Gene Ontology (GO) grouping using DAVID (Database for Annotation, Visualization and Integrated Discovery). The MNT's BNN20, BNN23, and BNN27 showed overlap of GO terms with NGF (nerve growth factor) and BDNF (brain-derived neurotrophic factor) in the H9eSC-derived MN's. In the iPSC-derived MN's two (BNN20, BNN27) showed overlap of GO terms with NGF or BDNF. Each NT protein had GO terms that did not overlap with any MNT in the MN cell lines.

1. Introduction

Amyotrophic lateral sclerosis (ALS) is a neurodegenerative disease (NDD) of adults first described in Western medicine by Charcot in the late 19th century [1]. ALS is usually rapidly fatal with death, in the absence of artificial ventilation, due to respiratory failure within 2–5 years of diagnosis. Pathologically, ALS develops from the accelerated dysfunction and death of upper and lower motor neurons, leading to spasticity, weakness, muscle atrophy, dysphagia and ventilatory failure.

Most ALS arises "sporadically" without known autosomal mutations (sporadic ALS, sALS), with ~5–10% of cases arising in families (familial ALS, fALS) from point mutations in at least 20 known genes or hexanucleotide expansions in the non-coding sequence between alternate 5′ exons in transcripts from C9orf72 [2,3]. This gene is associated with 9p-linked ALS and frontotemporal dementia (FTD [3,4]). Abnormally expanded C9orf72 is the most common known cause of fALS (~40%), is found in up to 11% of patients with sALS, and appears to interfere with RNA processing, export from the nucleus and protein translation [2–4].

There are no meaningful disease-altering therapies for sALS in spite of multiple large drug trials to determine efficacy. There are many potential reasons for these failures, including the possibility that sALS is a syndrome, like in many malignancies, where multiple different molecular genetic etiologies can yield similar clinical phenotypes. If true, then a search for a single universal therapy targeting one gene or pathway has limited chances for success, and a better approach could include drugs with pleiotropic effects on multiple neuronal survival pathways.

* Corresponding author at: Neurodegeneration Therapeutics, Inc., 3050A Berkmar Drive, Charlottesville, VA 22901, United States.
E-mail address: jim@neurodegenerationtherapeutics.comcastbiz.net (J.P. Bennett Jr.).
URL: http://www.NDTherapeutics.org (J.P. Bennett).

http://dx.doi.org/10.1016/j.bcp.2016.08.001
0006-2952/

Neurotrophins (NT's) may represent rational members of this therapeutic approach. NT's include multiple proteins endogenously produced in developing and/or adult nervous systems that promote neuronal growth and synapse formation, preservation of neuronal circuits, resistance to stress insults and inhibition of cell death [5]. NTs carry out these multiple actions by binding to and activating specific tyrosine kinase receptors (tropomyosin kinase, Trk) that auto-phosphorylate and activate cellular growth signaling [5–7]. Because they are large proteins, NT's are not good drug candidates for systemic administration to reach specific central nervous system (CNS) targets and have not shown efficacy in clinical studies of NDD's [5,6].

Microneurotrophins (MNT) are small molecule derivatives of dehydroepiandrosterone (DHEA), an endogenous steroid precursor with activity at sex hormone receptors. MNTs are devoid of sex hormone receptor activity but do bind potently to NT Trk receptors and show neurotrophic, anti-inflammatory and anti-apoptotic activities in multiple rodent neural cell, tissue and animal models [8–12].

There were two hypotheses tested in the present preclinical study. The first hypothesis was that MNT's would exhibit characteristics in *in vitro* or animal tests desirable of neurotherapeutics for ALS-would cross the blood–brain barrier (BBB), would lack significant ATP-binding cassette (ABC) transporter interaction and would exhibit slow metabolism by human liver.

The second hypothesis tested was that MNT's would behave at the molecular level similar to NT proteins.

To test the first hypothesis, we characterized *in vitro* the cell permeabilities, potential substrate activities of MNTs at the two human ABC transporters felt to account for removal ("reverse pumping") of drugs from the brain to blood across the BBB, metabolism by cryopreserved hepatocytes from mouse and human and crossing of the BBB in mice by a lead MNT BNN27. To test the second hypothesis, we used global gene expression analysis with RNA-sequencing (RNA-seq) to compare effects of MNT's and NT proteins in two sources of human stem cell-derived motor neurons.

2. Materials and methods

2.1. Generation of human iPSCs and motor neurons

The induced pluripotential stem cell (iPSC) cell line used was derived from peripheral blood mononuclear cells from a healthy donor using electroporation of pEB-C5 and pEB-Tg reprogramming plasmids ([13]; Addgene®) as described in O'Brien et al. [14]. H9-derived human embryonic neural stem cells (H9eSC, Gibco, Life Technologies) and iPSCs were differentiated into motor neurons following a previously described protocol [15] with modifications [14]. All cultures were maintained at 37 °C in reduced (5%) oxygen and 5% CO_2 conditions.

2.2. Incubation of differentiated motor neurons with MNTs or NTs

Following 21 days of motor neuron differentiation, cells were incubated with 100 nM BNN20, BNN23, or BNN27 (all in 0.001% dimethylsulfoxide (DMSO)), 0.001% DMSO vehicle control (Sigma-Aldrich, St. Louis, MO), 100 ng/ml nerve growth factor (NGF, Sigma-Aldrich) or 100 ng/ml brain-derived neurotrophic factor (BDNF, Sigma-Aldrich). MNTs were dissolved in DMSO and diluted; final DMSO was 0.001%. RNA was isolated using the RNeasy Plus Micro Kit (Qiagen, Valencia, CA) according to manufacturer instructions. Structures for the MNTs are shown in Fig. 1. These three MNT analogs were the first ones synthesized and characterized [10,11] and were kindly made available to us by Dr. A. Gravanis. At the time of manuscript preparation, no other MNT analogs had been synthesized.

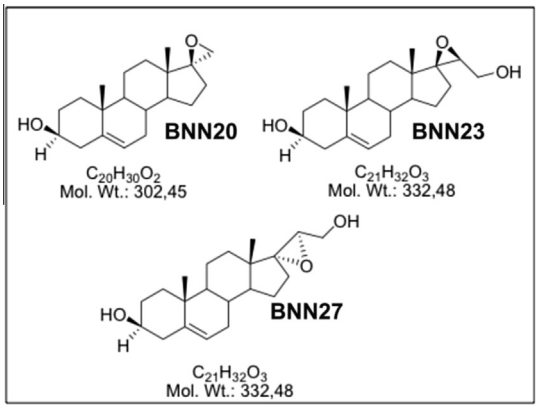

Fig. 1. Structures and MW's of the MNT's used in this study.

2.3. Sample preparation and sequencing

RNA for all samples was quantified using a Nanodrop® 2000c spectrophotometer (ThermoFisher Scientific, Waltham, MA) and quality was assessed using the Experion® automated electrophoresis system (Bio-Rad, Hercules, CA). Bio-Rad's Experion® calculated an RNA Quality Index (RQI) score by comparing three portions of a sample's electrophoretic profile to a manufactured standard of degraded RNAs. RNA Quality Index (RQI) values range between 1 and 10, with increasing values representing higher quality RNA. 500 ng of RNA from each sample with an RQI score $\geqslant 7$ was used for library construction.

The Illumina Truseq® Stranded Total RNA HT Sample Prep Kit® (Illumina, San Diego, CA) instructions were followed to generate barcoded RNA-Sequencing libraries for all eligible samples. We confirmed libraries had the expected sized band (~260 bp) using the Experion® automated electrophoresis system (Bio-Rad). We then quantified libraries using the KAPA® library quantification kit (Kapa Biosystems, Wilmington, MA). Barcoded RNA-Sequencing libraries were equimolar pooled and added to the Illumina Nextseq 500® lane for multiplex sequencing at Cofactor Genomics® (Saint Louis, MO). Data were processed using the standard Illumina processing pipeline to segregate each multiplexed sample's reads, and raw FastQ files for each sample were sent to us for further processing. We routinely obtained >50 million 2×150 base pair (bp), paired-end reads from each sample.

2.4. Data pre-processing and alignment with Tophat

FastQ files for each individual sample were input to FastQC (http://www.bioinformatics.babraham.ac.uk/projects/fastqc/) for quality assessments. This software identifies any data quality issues across metrics including: base quality per position across reads, overall GC content, sequence length distribution, and duplicate read frequency. All samples passed this QC check (data not shown).

Samples were next processed using Trimmomatic [16]. Trimmomatic removed all Illumina adaptor sequences and bases with a Phred quality score greater than 20 from the 3′ end of our reads. A Phred score of 20 indicates a 99% probability the base is correctly identified. Fragments > or = to 50 bp were retained after that step. We took these filtering steps to ensure high quality reads were used for alignment, as the average Phred score decreased in bases

toward the 3′ end of reads across samples decreased (data not shown).

We next used the Burrows-Wheeler Aligner (BWA [17]), to calculate insert size metrics for each sample (including average size and standard deviation) to improve Tophat2 alignment. Once these metrics were obtained, we aligned each sample's reads to the hg38 human reference transcriptome then genome using Tophat2 [18]. The hg38 reference transcriptome and genome were derived from Illumina iGenomes UCSC hg38 directory (https://support.illumina.com/sequencing/sequencing_software/igenome.html).

2.5. Cufflinks for gene abundance estimates

Gene and transcript abundances for all samples were estimated using Cufflinks v2.2.1 (http://cufflinks.cbcb.umd.edu/howitworks.html). We opted to mask all rRNA, tRNA, and mitochondrial RNA mapped reads from FPKM calculations, as these RNA species accounted for different proportions of total mapped reads in each sample. We only considered reads aligning to known genes (compatible hits norm flag) in our FPKM calculations, as we suspected the number of novel transcripts varies across samples. We also used the genome bias and multi-hits correction flags, as recommended by the Tuxedo Suite developers.

2.6. Determination of P-gp substrate properties of microneurotrophin drugs (Cyprotex®, Watertown, MA Table 1)

Madin Darby Canine Kidney (MDCK) epithelial cells stably transfected with the human *MDR1* gene (the gene encoding for the efflux protein P-glycoprotein, P-gp) are seeded on a Multiscreen™ plate (MilliporeSigma, Billerica, MA) and form a confluent monolayer over 4 days prior to the experiment. To verify the MDCK-MDR1 cell monolayers are properly formed, aliquots of the cell buffers are analyzed by fluorescence to determine the transport of the impermeable dye Lucifer Yellow. Any deviations from control values are reported.

For apical to basolateral (A → B) permeability, the test agent in the absence or presence of 100 μM verapamil (a P-gp inhibitor) was added to the apical (A) side and the amount of permeation is determined on the basolateral (B) side; for basolateral to apical (B → A) permeability, the test agent in the absence and presence of 100 μM verapamil was added to the B side and the amount of permeation was determined on the A side. The A-side buffer contains 100 μM Lucifer yellow dye, in Transport Buffer (1.98 g/L glucose in 10 mM HEPES, 1× Hank's Balanced Salt Solution) pH 7.4, while the B-side buffer has Transport Buffer at pH 7.4. MDCK-MDR1 cells are incubated with these buffers for 2 h, and the receiver side buffer is removed for analysis by LC–MS/MS (using propranolol as an analytical internal standard).

The rate of passage of the test compounds through this cell monolayer barrier from apical to basolateral (A → B) in this bi-directional transport assay is used to determine the apparent permeability coefficient (*Papp*) = (dQ/dt)/(C_0A) where dQ/dt is rate of permeation, C_0 is initial concentration of test agent, and A is the area of monolayer (0.11 cm^2).

The basolateral to apical (B → A) to apical to basolateral (A → B) apparent permeability coefficient ratio

$$R_e = \frac{P_{app}(B \rightarrow A)}{P_{app}(A \rightarrow B)}$$

is used to determine the extent of efflux of the test compounds. All experiments were carried out in duplicate and averaged results are shown.

2.7. Determination of BBB-PAMPA permeability properties of microneurotrophin drugs (Cyprotex®, Table 2)

Compounds (10 mM) in 100% DMSO were dissolved in transport buffer (pH 7.4) to a final concentration of 10 μM (final DMSO = 0.1%). The filter membrane was coated with 4 μl of a 20 mg/ml porcine brain lipid in dodecane. Three hundred (300) μl of the compound solution was added to the donor well. The acceptor well was filled with 200 μl of transport buffer. The acceptor filter plate was carefully placed on to the donor plate to create a sandwich. The plate was left undisturbed for 18 h. Samples of the donor and acceptor wells were analyzed by LC/MS/MS and the effective permeability (Pe) was calculated using the following equation: Data are expressed as permeability (*Pe*):

$$\log Pe = \{-((V_D V_A)/(V_D + V_A)At)\ln\{1 - [drug]_A/[drug]_E\}\}$$

where *Pe* is the permeability, V_D and V_A are the volumes of the donor and acceptor compartments, *A* is the area of the membrane, *t* is the incubation time, and *A* and E subscripts on the concentration term refer to the acceptor and equilibrium concentrations, respectively. All experiments were performed in quadruplicate and averaged results are shown.

Table 1
MDCK-MDR1 Permeability and P-gp Substrate Identification.

Test Article	Test Conc.	Assay Duration	Mean A → B P_{app} (10^{-6} cm s^{-1})	Mean B → A P_{app} (10^{-6} cm s^{-1})	Efflux Ratio	Comment
Ranitidine	10 μM	2 h	0.22	2.1	9.5	Low permeability
Warfarin	10 μM	2 h	28.2	35.1	1.2	High permeability
Loperamide	10 μM	2 h	1.1	71.9	65.4	P-gp efflux control
Loperamide + 100 μM verapamil	10 μM	2 h	46.6	48.4	1.1	P-gp substrate + inhibitor
BNN-20	10 μM	2 h	3.3	8.0	2.4	
BNN-20 + 100 μM verapamil	10 μM	2 h	4.4	10.7	2.4	BNN-20 is not a P-gp substrate*
BNN-27	10 μM	2 h	9.2	33.7	3.7	
BNN-27 + 100 μM verapamil	10 μM	2 h	9.6	39.5	4.1	BNN-27 is not a P-gp substrate
BNN-23	10 μM	2 h	7.6	30.7	4.0	
BNN-23 + 100 μM verapamil	10 μM	2 h	8.7	57.3	6.6	BNN-23 is not a P-gp substrate*

Papp: apparent permeability rate coefficient; Efflux Ratio: Papp (B → A)/Papp (A → B)
Conclusion: All 3 drugs exhibit moderate (or moderate-high) permeability rates across MDR1-MDCK epithelial monolayers with only minor efflux evident. The inclusion of verapamil did not alter this minor efflux.
* Low post-assay recovery in the A → B transport direction; Low recovery may be due to low aqueous solubility, high lipophilicity, and/or non-specific binding of the test article.

Table 2
BBB-PAMPA Permeability.

Test Article	Assay Duration	Mean Pe* ($x10^{-6}$ cm s^{-1})	Recovery (%)	Comment
Atenolol	18 h	0.0000	111	Low permeability control
Verapamil	18 h	34.9	42.2	High permeability control
BNN-20	18 h	7.9	35.4	High permeability
BNN-27	18 h	12.7	93.0	High permeability
BNN-23	18 h	14.0	94.3	High permeability

Pe*: Effective Permeability coefficient.
Conclusion: All 3 drugs exhibit high permeability rates across PAMPA-BBB membranes, predicting a high probability of passive BBB permeability.

2.8. Determination of breast cancer resistance protein (bcrp) properties of microneurotrophin drugs (Cyprotex®, Table 3)

Caco-2 cells (human epithelial colorectal adenocarcinoma cells) grown in tissue culture flasks are trypsinized, suspended in medium, and the suspensions were applied to wells of a Millipore 96 well Caco-2 plate. The cells are allowed to grow and differentiate for 21 days. For Apical to Basolateral (A → B) permeability, the drug is added to the apical (A) side and amount of permeation is determined on the basolateral (B) side; for Basolateral to Apical (B → A) permeability, the drug is added to the B side and the amount of permeation is determine on the A side. To verify a compound is a BCRP substrate, 50 μM of novobiocin is added to both chambers during the equilibration step and for the duration of the assay. The A-side buffer contains 100 μM Lucifer yellow dye, in Transport Buffer (1.98 g/L glucose in 10 mM HEPES, 1× Hank's Balanced Salt Solution) pH 7.4, and the B-side buffer is Transport Buffer, pH 7.4. Caco-2 cells are incubated with these buffers for 2 h, and the receiver side buffer is removed for analysis by LC–MS/MS. To verify the cell monolayers are properly formed, aliquots of the cell buffers are analyzed by fluorescence to determine the transport of the impermeable dye Lucifer Yellow. Any deviations from control values are reported.

Data are expressed as permeability P_{app}

$$P_{app} = \frac{dQ/dt}{C_0 A}$$

where dQ/dt is rate of permeation, C_0 is initial concentration of test agent, and A is the area of monolayer. All experiments were performed in duplicate and averaged results are shown.

2.9. In vitro and in vivo metabolism of BNN27

In vitro metabolism of BNN27 was carried out using cryopreserved hepatocytes from mice or humans. BNN27 was incubated in duplicate with primary, cryopreserved hepatocytes at 37 °C. The cells were thawed; viable cells counted, and equilibrated according to the supplier's directions. After 30 min equilibration at 37 °C with gentle agitation, BNN27 was added into the cell suspension to give the desired final concentration of 3 μM. The cell suspension was incubated at 37 °C as described above. At the indicated times, samples were removed and mixed with an equal volume of ice-cold stop solution (methanol). In parallel, blank hepatocytes in the absence of BNN27 was incubated for 120 min and is used as a control to show the presence of peaks derived from the hepatocytes. Stopped reactions were incubated at least ten minutes on ice, and an additional volume of water was added. The samples are centrifuged to remove precipitated protein, and the supernatants were analyzed by LC–MS/MS.

In vivo brain penetration and metabolism studies of BNN27 used adult CD-1 mice (n = 4) given 50 mg/kg IP of BNN27 dissolved in 10% DMSO; 90% of 10% hydroxypropyl-β-cyclodextrin in water. 30 min after injection the brains were removed and divided in half sagitally. One set of brain samples was homogenized in PBS buffer (2 ml per gram of tissue, on ice) and homogenates were mixed with 3 volumes of methanol containing an analytical internal standard (diclofenac) to extract the compound. Samples were centrifuged to remove precipitated protein and supernatants analyzed by LC–MS/MS. The second set of brain samples was homogenized in ice-cold absolute ethanol (2 ml per gram of tissue) and then stored overnight at −20 °C to extract. The following day, 3 volumes of methanol containing an analytical internal standard (diclofenac) was added, and samples were vortexed and centrifuged to remove precipitated protein, followed by LC–MS/MS analysis of the supernatants.

The analyte signal was optimized for each compound by electrospray ionization (ESI) in positive ionization mode. An MS2 scan was used to optimize the precursor ion mass, and an SIM scan was used to optimize the fragmenter voltage. Product ion analysis was used to identify the best fragment and collision energy for analysis. Following MRM method optimization, a test injection was performed using the column/gradient conditions shown below. A qualitative ionization ranking was assigned indicating the compound's ease of ionization.

Samples were analyzed by LC–MS/MS using a SCIEX QTrap 5500 mass spectrometer coupled with an Agilent 1290 HPLC Infinity ser-

Table 3
Caco-2 Cell Permeability and BCRP Substrate Identification.

Test Article	Test Conc.	Assay Duration	Mean A → B P_{app} (10^{-6} cm s^{-1})	Mean B → A P_{app} (10^{-6} cm s^{-1})	Efflux Ratio	Comment
ranitidine	10 μM	2 h	0.46	3.0	6.5	Low permeability ctl
warfarin	10 μM	2 h	21.5	16.2	0.75	High permeability ctl
Estrone 3-sulfate	10 μM	2 h	0.52	18.2	35.0	BCRP efflux control
Estrone 3-sulfart + 50 μM novobiocin	10 μM	2 h	2.2	2.2	1.0	BCRP substrate + inhibitor
BNN-20	10 μM	2 h	1.7	3.7	2.2	
BNN-20 + 50 μM novobiocin	10 μM	2 h	2.2	2.0	0.90	BNN-20 is not a BCRP substrate*
BNN-27	10 μM	2 h	4.0	6.0	1.5	
BNN-27 + 50 μM novobiocin	10 μM	2 h	6.4	3.3	0.52	BNN-27 is not a BCRP substrate*
BNN-23	10 μM	2 h	1.9	3.7	1.9	
BNN-23 + 50 μM novobiocin	10 μM	2 h	3.0	4.6	1.5	BNN-23 is not a BCRP substrate*

Conclusion: All 3 drugs exhibit moderate permeability rates across Caco-2 epithelial monolayers with no efflux evident. The inclusion of novobiocin did not significantly alter the overall permeability profiles of these compounds.
* Low post-assay recovery in the A → B transport direction; Low recovery may be due to low aqueous solubility, high lipophilicity, and/or non-specific binding of the drug.

ies, a CTC PAL chilled autosampler, all controlled by Analyst software. After separation on a C18 reverse phase HPLC column (Acquity UPLC HSS T3, 1.8, 2.1 × 50 mm) using an acetonitrile-water gradient system, peaks were analyzed by mass spectrometry (MS) using ESI ionization in MRM mode. HPLC retention times (R_t) of metabolites varied within 5% or less from each other.

2.10. Data analysis

All graphs, curve fitting and statistical analyses were performed with GraphPad Prism® for Macintosh, v 5.0–7.0. All RNA seq bioinformatics processing was performed using Unix code on Macintosh OSX v.10× MacPro computers with 8 or 12 core processors and 64 GB RAM.

3. Results

3.1. MNT's show very good cell permeability and are not major substrates for blood–brain barrier ABC transporters

Tables 1–3 show that none of the three MNTs tested *in vitro* were major substrates for human ABC transporters P-gp [19–22] (Table 1) or BCRP [22,23] (Table 3). The efflux rates (B → A) of BNN20 and BNN27 were reduced <50% by inclusion of novobiocin, suggesting weak interaction with BCRP transporter.

All three MNTs had high cellular permeability in a PAMPA assay (parallel artificial membrane permeability assay) (Table 2) in which the movement of drugs through a lipid-rich artificial membrane is measured. The effective permeability coefficients (Pe) for the three MNT's tested ranged from 7.9 to 14.0 ($\times 10^{-6}$ cm/s), with the high permeability CTL (verapamil) having a Pe of 34.9, and the low permeability CTL having Pe of 0.00. These findings suggest that MNTs will cross the BBB rapidly and will not be pumped out of the brain by P-gp and will be pumped very little if at all by BRCP. Both are known ABC transporters active at the BBB.

3.2. The lead MNT BNN27 is rapidly metabolized by mouse hepatocytes but more slowly metabolized by human hepatocytes to likely single hydroxylation species

Fig. 2 shows that cryopreserved mouse hepatocytes rapidly metabolized BNN27 whereas human cryopreserved hepatocytes more slowly metabolized BNN27. Both experiments were carried out over 2 h. Fig. 3 shows metabolic profiling of BNN27 following incubation with mouse (upper) or human (lower) cryopreserved hepatocytes. The detection was carried out at a mass/charge (m/z) ratio of 331, which represents the parent drug (m/z = 315) + 16 to scan for possible single mono-oxidation (likely hydroxylation) metabolites. At least 7 metabolites of BNN27 were identified in mouse hepatocyte cultures, whereas 3–4 metabolites of BNN27 were found in human hepatocyte cultures at much lower levels (~5-fold) (metabolite M1 present at very low levels). The individual metabolites were not structurally identified in this study.

3.3. BNN27 and its metabolites can be detected in mouse brain 30 min after injection

Fig. 4 shows that within 30 min of IP injection (50 mg/kg) of BNN27, 6 mono-oxidation metabolites are detectable in mouse brain (n = 4 mice examined; shown are the results from mouse 2 which were very representative of the group). BNN27 levels in whole brain, assayed by LC/MS/MS at m/z of 315, 30 min after 50 mg/kg IP injection, were 8230 ± 1995 (SEM) ng/gm with PBS/methanol extraction, and 9856 ± 1719 (SEM) ng/gm with ethanol extraction.

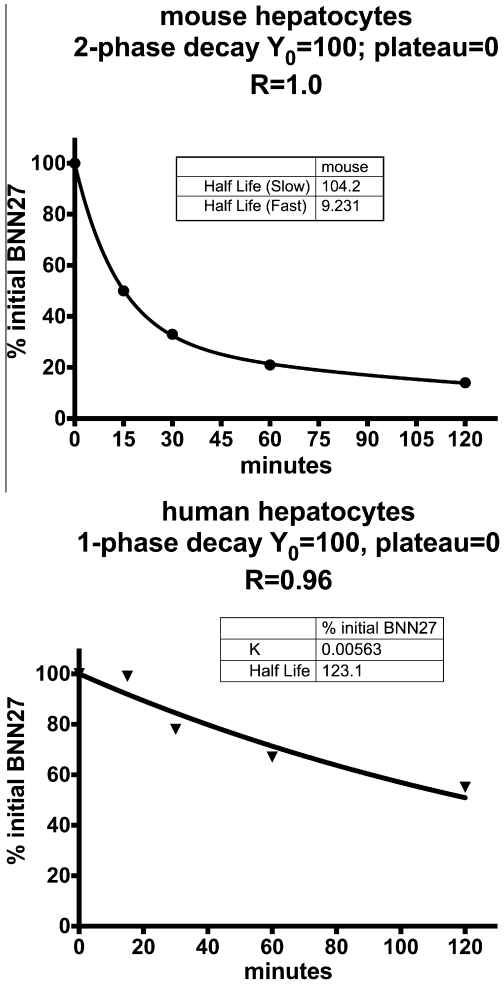

Fig. 2. BNN27 is metabolized rapidly by mouse cryopreserved hepatocytes (top) but more slowly by human cryopreserved hepatocytes (bottom). Experiments were carried out with 10 μM initial [BNN27] and at 37°. [BNN27] in the supernatant was analyzed by LC/MS/MS at m/z of 315. Data were fit to one- or two-phase decay curves in Prism®.

3.4. H9 eSC/NSC-derived motor neurons and Ctl iPSC/NSC-derived motor neurons have very similar gene expression

Fig. 5 shows that at the gene expression level, H9 eSC/NSC-derived motor neurons and Ctl iPSC/NSC-derived motor neurons were very similar to each other. There was an excellent correlation (Pearson r = 0.92) of the $\log_2$FPKM values for 8904 gene pairs from the two MN cell lines.

3.5. Gene expression analyses reveal many similarities among MNT's and NT's effects on NSC-derived motor neurons

We used Cufflinks2 to acquire FPKM (Fragments Per Kilobase of exon per Million reads) values in which NSC's made from H9 eSC/NSC's or iPSC's derived from PBMC's of a 62 year-old control individual without any neurological illness were differentiated into motor neurons for 21 days, then exposed in duplicate for 24 h to neurotrophin proteins (NGF, BDNF) at 100 ng/ml or MNT's BNN20, BNN23, BNN27 (see Fig. 1) at 100 nM, or to 0.001% DMSO vehicle. Total RNA was then extracted, analyzed for quality, barcoded sequencing libraries were made and quantitated, followed by multiplex, paired-end read RNA sequencing. The reads were checked for quality using FastQC®, trimmed of bar codes using Trimmomatic® [16], then aligned against the hg38 version of the

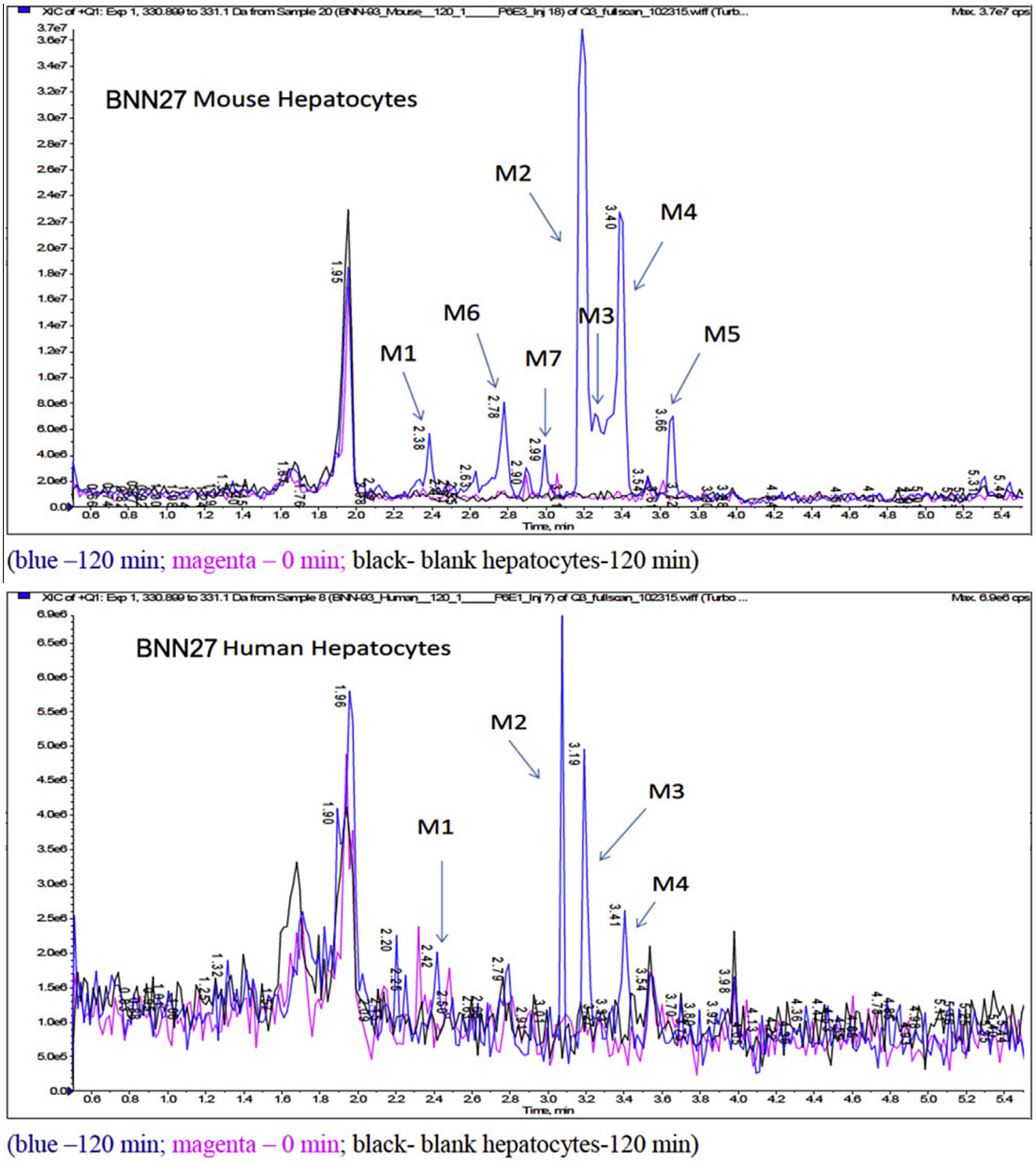

Fig. 3. Metabolism of BNN27 into mono-oxidation metabolites by mouse (top) and human (bottom) cryopreserved hepatocytes. Shown are LC/MS/MS tracing from *m*/*z* of 331 to detect mono-oxidation (likely hydroxylation) metabolites of BNN27 after 2 h of incubation with hepatocytes. Note that the relative levels of metabolites is ~5-fold less in human compared to mouse hepatocyte supernatants.

human genome using tophat2 [18]/bowtie2 (http://bowtie-bio.sourceforge.net/bowtie2/index.shtml), then quantitated using Cufflinks2 (http://cole-trapnell-lab.github.io/cufflinks/install/). The ratios of averaged FPKM values for each incubation condition divided by DMSO vehicle controls were ranked from largest to smallest. Genes from the top 500 ratios for each incubation condition were then submitted to DAVID and analyzed using gene annotation clustering.

Searching through the RNA-seq database of FPKM's showed that a number of neurotrophin-related genes were mildly stimulated by NT's or MNT drugs. Relative to expression in vehicle CTL (0.001% DMSO), the following genes were activated: ADCYAP1 (CRE-responsive): (BDNF 31%; BNN20 24%; BNN27 22%; BNN23 36%; NGF 35%); CREM (CREB modulator): (BDNF 27%; BNN20 -5%; BNN27 21%; NGF 3%); NRF2/NFE2L2 (Akt-responsive) (BDNF 13%; BNN20 1%; BNN27 -8%; BNN23 9.1%; NGF 0.5%). We also did observe that NRF1, not normally considered a neurotrophin-responsive gene was increased by BNN20 (28%); and BNN23 (38%). Notably, expression of thioredoxin (TXN), a major anti-oxidant gene considered to be stimulated by CREB, did not increase in the motor neurons following exposure to BDNF, NGF or any of the MNT drugs.

Tables 4 and 5 summarize our DAVID [32,33] findings after gene annotation clustering. We used a conservative strategy to report GO terms only and show only those GO terms with Benjamini (multiple comparison)-corrected p values <0.05.

For Table 4 (H9 eSC/NSC-derived MN's): Overall, the most significant GO term overlaps occurred with BNN20 and BNN27, and both NGF and BDNF, involving GO terms representing ribosome functions. The next most significant GO clustering involved BNN20 and BNN27, and NGF and BDNF, involving GO terms representing cytoskeleton. BNN23 showed significant GO term

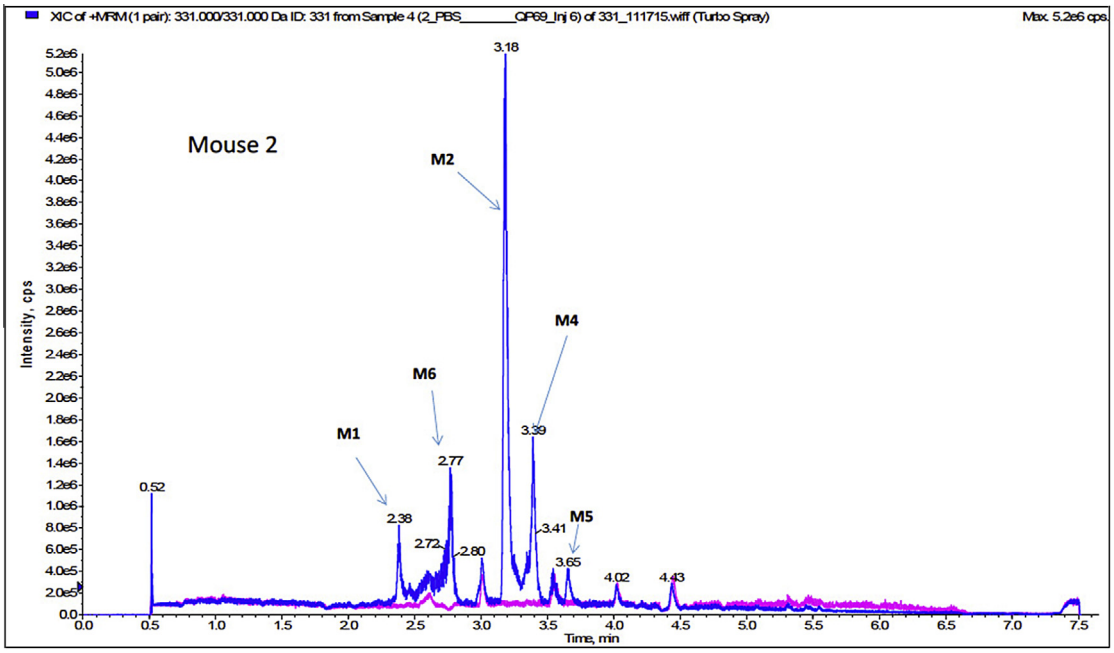

Fig. 4. Rapid entry of BNN27 mono-oxidation metabolites into CD-1 mouse brain (n = 4 mice studied) 30 min after systemic (IP) injection of BNN27 (50 mg/kg). Shown is the LC/MS/MS tracing of brain extract from mouse 2, revealing the presence of 6 out of the 7 mono-oxidation metabolites found in the mouse hepatocyte culture experiment (Fig. 4).

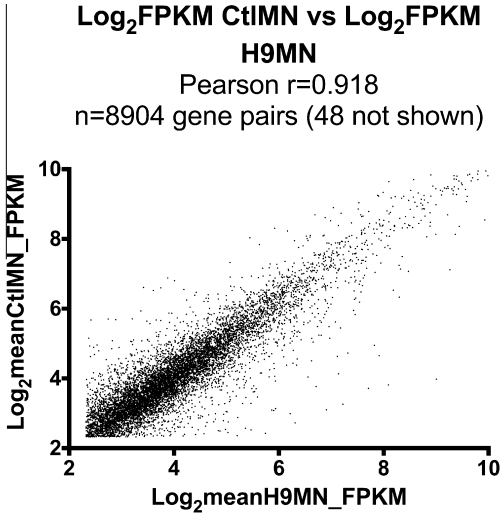

Fig. 5. Marked correlation in gene expression FPKM values between CTL-MN's and H9-MN's. Shown are results from 8904 gene pairs with minimum FPKM of 5.0. Data were taken from duplicate independent assays of RNAseq data from CTL-MN's and H9-MN's exposed to vehicle (0.001% DMSO) and are expressed as $\log_2$ of FPKM values. 48 points were outside the range of the graph.

alignment involving GO terms representing nucleoplasm and synaptic function, but these GO terms were not significantly represented by either neurotrophin protein or other MNT drugs. BNN27 shared one GO term involving intracellular and protein transport with NGF, and one GO term involving microtubule cytoskeleton that did not appear with either NT protein. Finally, each NT protein showed three GO terms each that did not appear with any MNT drug.

For Table 5 (Ctl iPSC/NSC-derived MN's): Overall the most significant GO term overlaps occurred with all three MNT drugs and both NT proteins in areas of cytoskeleton, organelle lumen and nuclear lumen. BNN20 and BNN23 showed GO term overlap with NGF in RNA splicing, translation and ribonucleoprotein complex. BNN20 and BNN27 showed GO term overlap with both NT's NGF and BDNF for intracellular organelle lumen, and all three MNT drugs showed GO term overlap with NGF in the area of growth cone formation and polarized growth. BNN20 by itself showed significant GO term clustering in areas of mitotic cell process and unfolded protein binding.

4. Discussion and conclusions

To date no cell or animal model of ALS accurately predicts efficacy of neuroprotective treatments for the most commonly occurring, sporadic form of the illness (sALS). Because of the survival-promoting, pleiotropic actions of neurotrophins on neurons [24], and the demonstrated efficacy of neurotrophins or neurotrophin receptors in preventing motor neuron death following axotomy [25–27], we are pursuing the pre-clinical development of microneurotrophins for ALS.

As part of this development effort, we characterized the *in vitro* permeability of the MNT's to artificial membrane and their interactions with ABC transporters that can remove drugs by reverse-pumping across the BBB. We observed that MNT's had excellent potential BBB permeability and were not major substrates for ABC drug transporters.

We then examined the metabolism of a lead MNT, BNN27, by mouse and human liver cells. We observed rapid metabolism by mouse and slower metabolism by human liver cells. In both systems BNN27 metabolites could be detected and are likely ring single hydroxylation metabolites produced by the cytochrome P450 system. However, because we did not characterize any of the metabolites structurally, we can only speculate as to their chemical identity.

Following systemic (IP) injection, BNN27 enters mouse brain within 30 min, but so do most of its mono-oxidation metabolites. This finding makes mouse experiments problematic in terms of assessing either efficacy or toxicity of BNN27, since the efficacious/offending species would not be clear. Because of the

Table 4
Gene Ontology (GO) Terms from DAVID for commercially acquired human H9 ESC-derived NSC's that were differentiated into motor neurons, then exposed to NGF or BDNF (100 ng/ml) or Microneurotrophins BNN20, BNN23, BNN27 (each at 100 nM) for 24 h and Analyzed by RNA Seq. X = present; En = range of GO enrichment (fold); Bj = range of Benjamini-corrected p values.

Gene Ontology (GO) terms	Nerve growth factor (NGF)	Brain-derived neurotrophic factor (BDNF)	BNN20	BNN23	BNN27
Ribosome, translation, ribonucleoprotein complex	X En 3.5–8.1-fold, Bj 0.045–4.7E−11	X En 2.6–6.9 Bj 0.05–0.01	X En 3.3–7.2 Bj 0.013–8.0E−6		X En 2.6–7.0 Bj 0.01–3.3E−7
Cytoskeletal part, non-membrane bound organelle	X En 1.6–1.7 Bj 0.01–4.8E−5	X En 1.4–1.8 Bj 0.03–0.01	X En 1.2–1.6 Bj 5.3E−4		X En 1.6 Bj 0.01–4.8E−5
Endoplasmic reticulum		X En 1.9–2.5 Bj 0.03–0.002	X En 1.0–2.0 Bj 0.03		
Nucleoplasm				X En 1.7 Bj 0.04	
Synapse				X En 2.6–3.0 Bj 0.01	
Microtubule cytoskeleton					X En 1.6–2.1 Bj 0.02–0.01
Intracellular transport, protein transport	X En 2.0–2.2 Bj 0.01				X En 2.2 Bj 0.02
Intracellular organelles	X En 1.5 Bj 0.04				
Growth cone, polarized growth	X En 5.8–5.9 Bj 0.04				
Spliceosome, small ribonucleoprotein complex	X En 3.4–9.5 Bj 0.04				
Vesicle, coated vesicle, vesicle membrane		X En 2.8–6.0 Bj 0.047–0.002			
Sterol/cholesterol biosynthesis		X En 9.2–10.8 Bj 0.03			
Golgi membrane		X En 2.8 Bj 0.047			

specificity of MS/MS detection, it is possible to distinguish among BNN27 parent drug ($m/z = 315$) and BNN27 mono-oxidation metabolites ($m/z = 331$) in hepatocyte supernatants and brain extracts. However, it is problematic to use mice for studies of BNN27 in brain, as the metabolites are rapidly formed after systemic injection and can be found in brain extracts.

We then examined the ability of three MNT drugs to activate gene programs in "young" motor neurons produced by differentiation of human neural stem cells produced from either human embryonic stem cells (hESC) or CTL human PBMC induced pluripotential stem cells (CTL iPSC). We carried out high-resolution, paired-end read RNA sequencing of libraries prepared from each MN cell type following incubation with either NT protein or MNT drug, and subjected the resulting lists of the 500 most activated genes (relative to DMSO control) to analysis in DAVID to determine GO groups. We used a conservative analysis of DAVID results and report only GO groups where the multiple comparison-corrected p values (by Benjamini method) were <0.05.

We found that in the CTL iPSC/NSC-derived MN's, all three MNT drugs stimulated the same GO groups as did NGF and BDNF, whereas in the H9 human eSC/NSC-derived MN's, two of the three MNT drugs activated similar GO groups as did NGF and BDNF. There were notable exceptions to these trends, and the "fit" is not perfect.

These studies point to the challenges in using "young" motor neurons that were differentiated from NSC's. We agree with the cautions advanced in a recent review of stem cell models of ALS [31]. We have found that increasing duration of MN differentiation from 21 days to 42 days substantially increases neurophysiological maturity (depolarization spikes following current injection) (O'Brien et al., under review). We do not yet know to what extent neuromuscular synapse formation among iPSC-derived MN's and muscle cells, presence of co-cultured astrocytes, or growth in a 3-D scaffold matrix will alter MN gene expression following NT or MNT exposure. These are conditions to be explored in future studies.

Because it is not clear which GO terms are most involved in MN dysfunction and death in ALS, it is not possible to select any one MNT drug based on the results shown in Tables 4 and 5. Rather, it seems reasonable to conclude that the MNT drugs tested are capable of stimulating many of the same GO families as do NT proteins in the MN cell lines.

There are many limitations to our study:

First, the RNA sequencing bioinformatics analyses have inherent biases [28], particularly with the Cufflinks quantitation of gene expression that in our experience overestimates gene expression relative to other approaches such as DEseq [29] or EdgeR [30].

Table 5
Gene Ontology (GO) terms from DAVID for CTL human iPSC/NSC-derived motor neurons exposed to NGF or BDNF (100 ng/ml) or microneurotrophins BNN20, BNN23, BNN27 (each at 100 nM) for 24 h and analyzed by RNA seq. X = present; En = range of GO enrichment (fold); Bj = range of Benjamini-corrected p values.

Gene Ontology (GO) terms	Nerve growth factor (NGF)	Brain-derived neurotrophic factor (BDNF)	BNN20	BNN23	BNN27
RNA splicing, translation, ribonucleoprotein complex	X En 2.3-fold, Bj 0.003		X En 2.4–4.6 Bj 0.038–4.1E−6	X En 2.3 Bj 0.007	
Cytoskeletal part, non-membrane bound organelle	X En 1.6–3.2 Bj 0.01–1.2E−5	X En 1.5 Bj 0.002	X En 1.6 Bj 1.9E−4	X En 1.5 Bj 0.009	X En 1.5 Bj 0.018
Organelle lumen, membrane-enclosed lumen nuclear lumen	X En 1.8 Bj 2.0E−4–4.5E−5	X En 1.8–1.9 Bj 1.2E−5–3.3E−6	X En 1.9–2.0 Bj 0.038–7.5E−6		
Microtubule cytoskeleton	X En 2.2 Bj 0.003			X En 1.6–1.7 Bj 0.01–0.006	X En 1.6 Bj 0.03–0.02
Intracellular organelle lumen	X En 1.8 Bj 2.7E−5	X En 1.9 Bj 3.3E−6	X En 1.9 Bj 2.8E−6		X En 1.6–2.1 Bj 0.02–0.01
Growth cone, polarized growth	X En 6.9–7.0 Bj 0.002		X En 5.5–5.6 Bj 0.046–0.043	X En 1.7 Bj 0.006	X En 1.6 Bj 0.029
Neuron projection	X En 2.7 Bj 0.003				
Chromosome, chromatin	X En 2.1–2.9 Bj 0.02–0.008				
Mitotic cell cycle, cell cycle process/phase			X En 2.4–2.7 Bj 0.03–0.01		
Unfolded protein binding			X En 5.1 Bj 9.4E−4		

Second, we examined only two MN cell lines, whereas a greater number of lines, particularly some from ALS subjects, would have increased the generalizability of our findings.

Third, we examined gene expression changes after 24 h of NT or MNT exposure. We do not know if longer periods of incubation would have activated (or repressed) gene programs.

Fourth, we did not use a FACS-concentrated population of MN's. It is likely that some of the cells studied are "young" neurons but not yet differentiated to "young" MN's.

And fifth, and perhaps most important, we do not yet have any follow-up data on the actual efficacy of any MNT in ALS subjects. This awaits clinical studies of one or more MNT drugs in humans with ALS.

In spite of these limitations, we do conclude that our findings, although limited in interpretation, support going forward with MNT development. Our finding that MNT's activate gene programs similar to NT proteins, in two human, derived MN cell lines, suggest that MNT drugs will mimic NT actions on spinal MN's in ALS subjects. Clinical trials will be necessary to determine MNT efficacy, but our findings that 100 nM levels of MNT can activate gene programs in "young" MN's is encouraging for achieving these drug levels *in vivo*.

Ethics statement

All of the human investigation procedures (blood drawing) described in this study were approved by the Virginia Commonwealth University Institutional Review Board (VCU-IRB). All subjects provided informed consent by signing in the presence of witnesses a VCU-IRB-approved Consent form. Blood samples were coded at the time of collection to remove all patient identifiers and were processed in their coded forms. The iPSC and NSC cell lines used in this study had already been prepared before this study was undertaken. All vertebrate animal studies reported were carried out with IACUC approval by Avastus, Inc., a Massachusetts-based CRO that has been approved by the NIH Office of Laboratory Animal Welfare. (OLAW; Assurance renewal # A4543-01)

Conflict of interest statement

None of the authors has any personal financial interest in microneurotrophin drugs or BioNature. No conflicts of interest are declared.

Author contributions

JPB, DGB, and LCO designed experiments. DGB and LCO carried out experiments and derived primary data. DGB and LCO carried out all stem cell experiments. DGB and JPB analyzed RNAseq data. JPB wrote the paper, which was edited by DGB and LCO. All authors have read and agree with the final version.

Funding

This research was supported by ALS Worldwide and the VCU Parkinson's and Movement Disorders Center. Sponsors had no role

in experimental design, data analysis, manuscript preparation or decision to publish.

Acknowledgements

The authors thank Ms. Paula Keeney for assistance with cell culture, Drs. A. Gravanis and C. Neophytou for providing the three MNT analogs tested, colleagues at CoFactor Genomics® for carrying out the Illumina RNA sequencing, and Dr. B. Press and colleagues at Cyprotex® for carrying out the permeability, ABC transporter and BNN27 metabolism assays. Primary RNA sequencing data are deposited at NCBI's Sequence Read Archive (SRA) under the study accession number SRP064478.

References

[1] A. Al-Chalabi, O. Hardiman, The epidemiology of ALS: a conspiracy of genes, environment and time, Nat. Rev. Neurol. 9 (2013) 617–628.
[2] A.E. Renton, A. Chio, B.J. Traynor, State of play in amyotrophic lateral sclerosis genetics, Nat. Neurosci. 17 (2014) 17–23.
[3] M. Prudencio, V.V. Belzil, R. Batra, C.A. Ross, T.F. Gendron, L.J. Pregent, et al., Distinct brain transcriptome profiles in C9orf72-associated and sporadic ALS, Nat. Neurosci. 18 (2015) 1175–1182.
[4] A. Jovicic, J. Mertens, S. Boeynaems, E. Bogaert, N. Chai, S.B. Yamada, et al., Modifiers of C9orf72 dipeptide repeat toxicity connect nucleocytoplasmic transport defects to FTD/ALS, Nat. Neurosci. 18 (2015) 1226–1229.
[5] J.P. Steiner, A. Nath, Neurotrophin strategies for neuroprotection: are they sufficient? J. Neuroimmune Pharmacol. 9 (2014) 182–194.
[6] I. Mocchetti, M. Brown, Targeting neurotrophin receptors in the central nervous system, CNS Neurol. Disord. Drug Targets 7 (2008) 71–82.
[7] I.G. Onyango, J.Y. Ahn, J.B. Tuttle, J.P. Bennett Jr., R.H. Swerdlow, Nerve growth factor attenuates oxidant-induced beta-amyloid neurotoxicity in sporadic Alzheimer's disease cybrids, J. Neurochem. 114 (2010) 1605–1618.
[8] I. Charalampopoulos, V.I. Alexaki, C. Tsatsanis, V. Minas, E. Dermitzaki, I. Lasaridis, et al., Neurosteroids as endogenous inhibitors of neuronal cell apoptosis in aging, Ann. N. Y. Acad. Sci. 1088 (2006) 139–152.
[9] I. Charalampopoulos, E. Remboutsika, A.N. Margioris, A. Gravanis, Neurosteroids as modulators of neurogenesis and neuronal survival, Trends Endocrinol. Metab. 19 (2008) 300–307.
[10] T. Calogeropoulou, N. Avlonitis, V. Minas, X. Alexi, A. Pantzou, I. Charalampopoulos, et al., Novel dehydroepiandrosterone derivatives with antiapoptotic, neuroprotective activity, J. Med. Chem. 52 (2009) 6569–6587.
[11] A. Gravanis, T. Calogeropoulou, V. Panoutsakopoulou, K. Thermos, C. Neophytou, I. Charalampopoulos, Neurosteroids and microneurotrophins signal through NGF receptors to induce prosurvival signaling in neuronal cells, Sci. Signal. 5 (2012). pt8.
[12] I. Pediaditakis, I. Iliopoulos, I. Theologidis, N. Delivanoglou, A.N. Margioris, I. Charalampopoulos, et al., Dehydroepiandrosterone: an ancestral ligand of neurotrophin receptors, Endocrinology 156 (2015) 16–23.
[13] S.N. Dowey, X. Huang, B.K. Chou, Z. Ye, L. Cheng, Generation of integration-free human induced pluripotent stem cells from postnatal blood mononuclear cells by plasmid vector expression, Nat. Protoc. 7 (2012) 2013–2021.
[14] L.C. O'Brien, P.M. Keeney, J.P. Bennett Jr., Differentiation of human neural stem cells into motor neurons stimulates mitochondrial biogenesis and decreases glycolytic flux, Stem Cells Dev. 24 (2015) 1984–1994.
[15] M.W. Amoroso, G.F. Croft, D.J. Williams, S. O'Keeffe, M.A. Carrasco, A.R. Davis, et al., Accelerated high-yield generation of limb-innervating motor neurons from human stem cells, J. Neurosci. 33 (2013) 574–586.
[16] A.M. Bolger, M. Lohse, B. Usadel, Trimmomatic: a flexible trimmer for Illumina sequence data, Bioinformatics (Oxford, England) 30 (2014) 2114–2120.
[17] H. Li, R. Durbin, Fast and accurate long-read alignment with Burrows-Wheeler transform, Bioinformatics (Oxford, England) 26 (2010) 589–595.
[18] D. Kim, G. Pertea, C. Trapnell, H. Pimentel, R. Kelley, S.L. Salzberg, TopHat2: accurate alignment of transcriptomes in the presence of insertions, deletions and gene fusions, Genome Biol. 14 (2013) R36. doi: 10.1186/gb-2013-14-4-r36.
[19] E.M. Leslie, R.G. Deeley, S.P. Cole, Multidrug resistance proteins: role of P-glycoprotein, MRP1, MRP2, and BCRP (ABCG2) in tissue defense, Toxicol. Appl. Pharmacol. 204 (2005) 216–237.
[20] D.S. Miller, Regulation of P-glycoprotein and other ABC drug transporters at the blood-brain barrier, Trends Pharmacol. Sci. 31 (2010) 246–254.
[21] A.L. Bartels, Blood-brain barrier P-glycoprotein function in neurodegenerative disease, Curr. Pharm. Des. 17 (2011) 2771–2777.
[22] S. Agarwal, A.M. Hartz, W.F. Elmquist, B. Bauer, Breast cancer resistance protein and P-glycoprotein in brain cancer: two gatekeepers team up, Curr. Pharm. Des. 17 (2011) 2793–2802.
[23] K. Natarajan, Y. Xie, M.R. Baer, D.D. Ross, Role of breast cancer resistance protein (BCRP/ABCG2) in cancer drug resistance, Biochem. Pharmacol. 83 (2012) 1084–1103.
[24] O. Schulte-Herbruggen, A. Braun, S. Rochlitzer, M.C. Jockers-Scherubl, R. Hellweg, Neurotrophic factors – a tool for therapeutic strategies in neurological, neuropsychiatric and neuroimmunological diseases? Curr. Med. Chem. 14 (2007) 2318–2329.
[25] S. Wiese, S. Jablonka, B. Holtmann, N. Orel, R. Rajagopal, M.V. Chao, et al., Adenosine receptor A2A-R contributes to motoneuron survival by transactivating the tyrosine kinase receptor TrkB, Proc. Natl. Acad. Sci. U.S.A. 104 (2007) 17210–17215.
[26] H.U. Saragovi, E. Hamel, A. Di Polo, A neurotrophic rationale for the therapy of neurodegenerative disorders, Curr. Alzheimer Res. 6 (2009) 419–423.
[27] S. Morcuende, R. Munoz-Hernandez, B. Benitez-Temino, A.M. Pastor, R.R. de la Cruz, Neuroprotective effects of NGF, BDNF, NT-3 and GDNF on axotomized extraocular motoneurons in neonatal rats, Neuroscience 250 (2013) 31–48.
[28] Z.H. Zhang, D.J. Jhaveri, V.M. Marshall, D.C. Bauer, J. Edson, R.K. Narayanan, et al., A comparative study of techniques for differential expression analysis on RNA-Seq data, PLoS One 9 (2014) e103207.
[29] M.I. Love, W. Huber, S. Anders, Moderated estimation of fold change and dispersion for RNA-seq data with DESeq2, Genome Biol. 15 (2014) 550.
[30] M.D. Robinson, D.J. McCarthy, G.K. Smyth, EdgeR: a bioconductor package for differential expression analysis of digital gene expression data, Bioinformatics (Oxford, England) 26 (2010) 139–140.
[31] S. Sances, L.I. Bruijn, S. Chandran, K. Eggan, R. Ho, J.R. Klim, et al., Modeling ALS with motor neurons derived from human induced pluripotent stem cells, Nat. Neurosci. 16 (2016) 542–553.
[32] W. Huang da, B.T. Sherman, R.A. Lempicki, Systematic and integrative analysis of large gene lists using DAVID bioinformatics resources, Nat. Protoc. 4 (2009) 44–57.
[33] W. Huang da, B.T. Sherman, R.A. Lempicki, Bioinformatics enrichment tools: paths toward the comprehensive functional analysis of large gene lists, Nucleic Acids Res. 37 (2009) 1–13.